Article

Discovery Medicine 2023; 35(178): 910–920
https://doi.org/10.24976/Discov.Med.202335178.86

Spatial Heterogeneity of Integrins and Their Ligands in Primary Breast Tumors

Liubov Tashireva[1,2], Evgeniya Grigoryeva[1,3,*], Vladimir Alifanov[1,2], Pavel Iamshchikov[4], Marina Zavyalova[2], Vladimir Perelmuter[2]

[1]The Laboratory of Molecular Therapy of Cancer, Cancer Research Institute, Tomsk National Research Medical Center, Russian Academy of Sciences, 634009 Tomsk, Russia
[2]The Department of General and Molecular Pathology, Cancer Research Institute, Tomsk National Research Medical Center, Russian Academy of Sciences, 634009 Tomsk, Russia
[3]The Laboratory of Molecular Oncology and Immunology, Cancer Research Institute, Tomsk National Research Medical Center, Russian Academy of Sciences, 634009 Tomsk, Russia
[4]The Laboratory of Cancer Progression Biology, Cancer Research Institute, Tomsk National Research Medical Center, Russian Academy of Sciences, 634009 Tomsk, Russia
*Correspondence: grigoryeva.es@gmail.com (Evgeniya Grigoryeva)
Published: 1 October 2023

Background: The diversity of cell-cell interactions in different regions of a tumor reflects the functional heterogeneity of cancer, which poses challenges in early diagnosis, selection of treatment strategies, and prognosis of breast cancer. Cancer cells interact with each other to form different morphological structures in the tumor and stromal host cells via integrins. The objective of this study was to characterize the morphological and spatial heterogeneity of primary breast tumors in the context of expression profiles of integrins and their ligands.
Methods: We studied spatial transcriptomics using the 10X Visium approach and the Niche Interactions and Communication Heterogeneity in Extracellular Signaling (NICHES) algorithm to map ligand-receptor signaling pathways and visualize the heterogeneity of signaling archetypes in tumor clusters.
Results: Cluster analysis of the expression profiles of tumor spots from the samples indicated pronounced inter-tumoral heterogeneity. Integrin-ligand functional clusters were associated with intratumoral heterogeneity, which was manifested by the presence of several morphological loci as observed in histological tumor samples. Inter-tumoral heterogeneity was manifested by a different number of functional clusters, ranging from 2 to 9 for each tumor sample. The main characteristic of these clusters was the significant predominance of non-complementary integrin subunits. Of the 42 functional integrin-ligand pairs in 21 clusters of five samples, 41 pairs occurred only once. The exception was the laminin subunit alpha-5 (*LAMA5*)-integrin beta 4 (*ITGB4*) pair, which was detected in two clusters of different samples.
Conclusions: The spatial heterogeneity of integrin-ligand expression clusters in breast cancer contributes significantly to the functional heterogeneity of the tumor, which sets the stage for many scenarios of parenchymatous-stromal relationships, some of which may be effective in the emergence of metastasizing tumor seed cells. The intra- and inter-tumoral spatio-functional heterogeneity of the tumor tissue that we discovered may largely explain why it is difficult to achieve success in most patients with breast cancer using any therapeutic strategy targeting one molecule of the vast array, regardless of the importance of its pathogenetic significance.

Keywords: tumor heterogeneity; spatial transcriptomics; breast cancer; cell adhesion

Introduction

Integrins, a ubiquitous family of $\alpha\beta$ heterodimeric receptors, engage in extensive interactions with various ligands in both physiological and pathological contexts. These receptors regulate crucial cellular processes, including growth, proliferation, migration, signaling, cytokine production and activation, apoptosis, and tissue repair, which are crucial for inflammation and angiogenesis [1]. Accumulating evidence strongly suggests that integrins are involved in almost all stages of tumor development [2]. Remarkably, not all tumor cells can invade and disseminate from the primary tumor to distant organs. Critical attributes that influence the metastatic potential of tumor cells include stem-like features and epithelial-mesenchymal transition (EMT) characteristics. The aforementioned properties and other relevant factors that influence tumor cell aggressiveness do not manifest equally in different cells of the primary tumor. This phenomenon illustrates intratumoral heterogeneity in breast cancer. Considerable tumor

heterogeneity poses challenges for early diagnosis, selection of treatment strategies, and prognosis of breast cancer. For instance, recurrence and distant metastases, as well as the ineffectiveness of breast cancer treatment, arise because of tumor heterogeneity [3,4]. Spatial heterogeneity describes the distribution and interactions of different cell populations in tumor structures [3]. Morphological heterogeneity in breast cancer describes the presence of five main types of invasive components in the tumor: tubular, alveolar, solid, and trabecular structures, and discrete groups of tumor cells, and is known to be associated with both disease prognosis and response to chemotherapy [5]. To date, there have been no investigations of the spatial heterogeneity of integrin ligand-receptor interactions in primary breast cancer.

Therefore, in the present study, we focused on characterizing the heterogeneity of luminal breast cancer associated with expression profiles of integrin and ligand, with respect to the morphological and spatial heterogeneity of the tumor.

Materials and Methods

Patient Samples and Ethics

The study included samples from five breast cancer patients (invasive carcinoma of nonspecific type, luminal A and B, stage I–IIA, grade 2–3). The ages of the patients ranged from 22 to 68 years. Formalin-fixed paraffin-embedded (FFPE) samples were used for spatial transcriptomic analysis. All patients underwent sectoral resection and intraoperative radiation therapy. Sentinel lymph node biopsies were performed during surgical treatment for all patients. After surgery, the patients received chemotherapy according to the National Comprehensive Cancer Network (NCCN) recommendations. During the three-year follow-up period, no progression of the disease was observed.

Assessment of RNA Quality, Sample Preparation, and Library Construction

To assess the quality of FFPE tissue blocks, RNA was extracted from 10 µm-thick sections using a PureLink FFPE RNA Isolation Kit (Thermo Fisher Scientific, Waltham, MA, USA) according to the manufacturer's recommendation. RNA quality was assessed based on the mean RNA fragment size and percentage of total RNA fragments >200 nucleotides using a High-Sensitivity RNA ScreenTape on a 4150 TapeStation (Agilent, Santa Clara, CA, USA). Five-micrometer sections of FFPE tissue blocks prepared using five breast tumor samples were mounted on visible spatial slides. The samples were deparaffinized, hematoxylin and eosin (H&E)-stained, visualized, and de-crosslinked according to a previously described protocol (CG000409|Rev B, 10x Genomics). Libraries were prepared using the Visium Spatial Gene Expression Reagent Kit (10X Genomics, Pleasanton, CA, USA) for FFPE (CG000407|Rev C). The concentrations of the cDNA libraries were measured using a dsDNA High-Sensitivity Kit (Q33230, Invitrogen™, Thermo Fisher Scientific, Waltham, MA, USA) and a Qubit 4.0 fluorometer (Thermo Fisher Scientific, Waltham, MA, USA). cDNA concentrations varied from 2.7 to 5.5 ng/µL. The quality of the cDNA libraries was assessed using a High-Sensitivity D1000 ScreenTape on a 4150 TapeStation. The peak size varied from 251 to 261 bp (Agilent, Santa Clara, CA, USA).

Sequencing

1.8 pM samples of libraries were loaded and sequenced using the NextSeq 500 System (Illumina, San Diego, CA, USA) as paired-end 150 bp reads according to the following read protocol: read 1, 28 cycles; i7 index read, 10 cycles; i5 index read, 10 cycles; and read 2, 50 cycles. The median sequencing depth was 28,153 read pairs per spot.

Data Processing

Raw sequencing reads were initially processed into barcode feature matrices using Space Ranger v.1.3 (10X Genomics, Pleasanton, CA, USA) with default parameters. The resulting barcode feature matrices were uploaded to the R environment using the Seurat [6] R package (https://www.R-project.org/). Samples were filtered based on genes with nonzero expression in fewer than 10 tissue spots and tissue spots with fewer than 200 filtered genes. Raw counts were normalized using the SCTransform [7] function with default parameters. Uniform manifold approximation and projection (UMAP) was applied to the SCTransform normalized counts using the first 30 principal components following principal component analysis (PCA). Clustering of tissue spots was performed using shared nearest neighbor (SNN) clustering using the first 30 principal components. Preprocessing was performed using the Seurat tool. The Niche Interactions and Communication Heterogeneity in Extracellular Signaling (NICHES) [8] R package was used to assess ligand-receptor interactions between neighboring tissue spots. To mitigate the dropout effect, an adaptively thresholded low-rank approximation (ALRA) [9] imputation on log-normalized counts was used. ALRA-imputed gene expression was used in Niche Interactions and Communication Heterogeneity in Extracellular Signaling NICHES analysis. The resulting matrices of ligand-receptor interactions were used to perform UMAP and SNN clustering to cluster tissue spots with similar signaling microenvironments. The FindAllMarkers function in Seurat was used to reveal the most significant ligand-receptor interactions in the individual ligand-receptor interaction clusters. The results were visualized using the Seurat package.

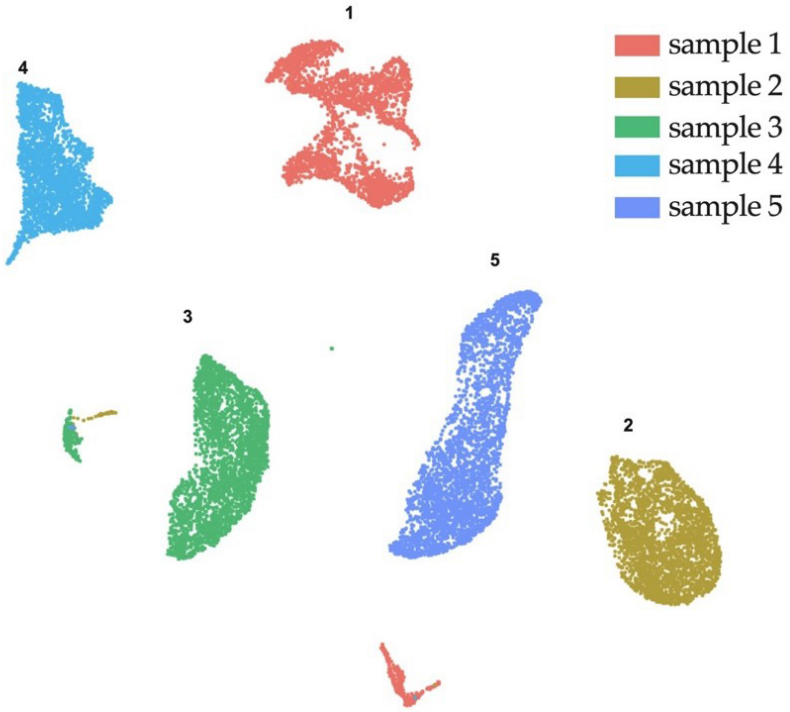

Fig. 1. The uniform manifold approximation and projection (UMAP) projection of the studied dataset colored according to tumor samples. The plot depicts spots of each sample belonging to different clusters. Numbers 1-5 correspond to patients' codes.

Results

Initial Data Characterization

To examine the spatial gene expression data, we first applied conventional normalization methods to visualize the data in two-dimensional space using UMAP (Fig. 1).

Cluster analysis of gene expression profiles in tumor spots from samples of different patients demonstrated separation into isolated clusters, with a high degree of divergence between patients. This clustering pattern indicated pronounced inter-tumor heterogeneity. In each spot (~0–20 cells/spots), multiple and diverse cell types were found to contribute to the transcriptional profile, resulting in variations in clustering across patients [10]. Thus, it was reasonable to analyze each sample separately.

Expression-Based Clustering of Individual Samples

Using the NICHES algorithm, a tool used to elucidate extracellular signaling at the single-cell level, we clustered each sample (Fig. 2). Next, we morphologically annotated each cluster and highlighted only the clusters in which tumor cells were represented. The spots in these clusters may include non-cancerous host stromal cells. All samples had more than one cluster labeled as tumors (**Supplementary Fig. 1**).

Cluster Annotation

NICHES cluster analysis showed pronounced intratumoral and inter-tumoral heterogeneity in the features studied. Table 1 summarizes all ligand-receptor pairs with integrins as receptors found via cluster analysis. For better comprehension of data, we combined the morphological characterization of the cluster with the characterization of the integrin profile of ligand-receptor interactions (Table 1, Ref. [11–33]).

Trabecular structures were predominant in spots corresponding to cluster 0 in sample 1. The tumor-stroma ratio was evaluated according to the recommendations of the International Immuno-Oncology Biomarker Working Group on Breast Cancer (2018) and was 1:1 [34]. Infiltration of the stroma by mononuclear cells within the cluster was approximately 5–10%. Cluster 0 was characterized by integrin alpha 6 (*ITGA6*) expression, which was associated with three ligands: thrombospondin 1 (*THBS1*), midkine (*MDK*), and laminin subunit gamma-1 (*LAMC1*). *THBS1* encodes thrombospondin 1, which mediates intercellular interactions; binds to fibrinogen, fibronectin, laminin, and collagen types V and VII; and plays a role in angiogenesis. In the spots corresponding to cluster 3, small solid structures were observed, and the tumor-stroma ratio was 5:1. Infiltration of the stroma by mononuclear cells within the cluster was approximately 5%. Genes of the Milk fat globule-EGF factor 8 (*MFGE8*)-integrin beta 3 (*ITGB3*) ligand-receptor pair were detected in cluster 3. MFGE8 protein (lactadherin) is known to bind integrins $\alpha v\beta 3$ and $\alpha v\beta 5$ on phagocytic cells for opsonization of apoptotic cells and uptake of dead cells [14]. Trabecular and torpedo-like structures prevailed in the spots corresponding to cluster

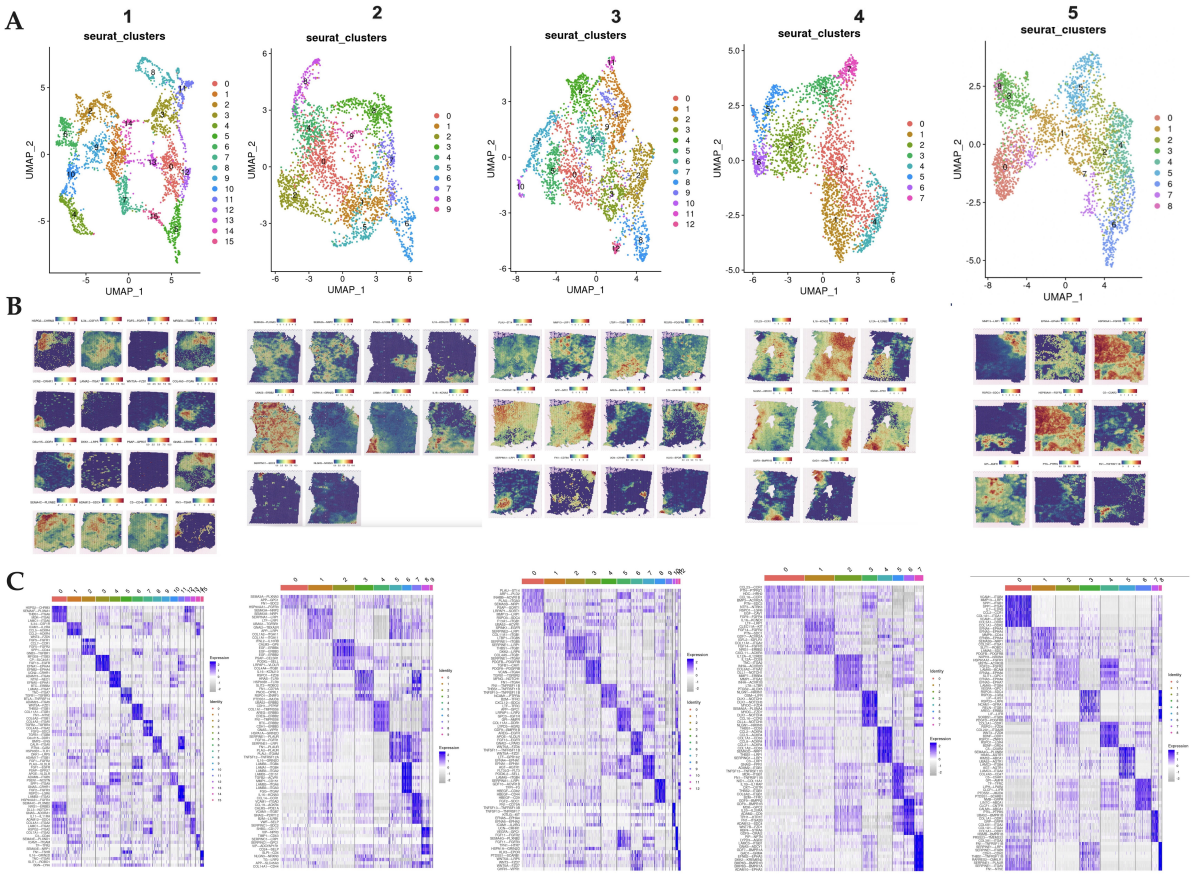

Fig. 2. Niche Interactions and Communication Heterogeneity in Extracellular Signaling (NICHES) analysis of primary breast tumors. (A) UMAP projection of clusters of each sample demonstrates high diversity. (B) Heat map projection of Top-1 overexpressed ligand-receptor pairs in different clusters obtained from different tissue slides. Visualization allows the correlation of expression characteristics of spots with the morphology of histological tissue slices. (C) List of overexpressed ligand-receptor pairings from corresponding clusters. Notably, not every cluster contains integrin-ligand pairings.

7; the tumor-to-stroma ratio was 1:1. The infiltration of the stroma by mononuclear cells within the cluster was approximately 20%. Cluster 7 was characterized by the RNA expression of three integrin subunits and their corresponding ligands: collagen alpha-3(IV) chain (*COL4A3*)-*ITGAV*, *COL4A3*-*ITGA2*, and *TGFB2*-*ITGB8*. The protein products of *ITGAV* and *ITGA2* could potentially bind to the product of *COL4A3* in this cluster, a constituent of type IV collagen and a major structural component of basal membranes. The spots of cluster 8 were found in two regions: the first was smaller, with a predominance of small solid structures with a tumor-stroma ratio of 1:1 and tumor-infiltrating lymphocytes (TILs) infiltration of approximately 5%. The second was represented by solid structures with a tumor-stroma ratio of 10:1. Cluster 8 was characterized by calreticulin (*CALR*)-*ITGAV* pairing. In the tumor locus corresponding to cluster 9, the spots were located predominantly within small solid structures. The tumor-to-stroma ratio within the cluster was 5:1, and TIL infiltration was approximately 20%. Cluster 9 showed the expression of only one *ITGB1* subunit and a potential disintegrin and metalloproteinase domain 17 (*ADAM17*) ligand, which encodes a metalloprotease enzyme whose primary role is to cleave the membrane fragment of tumor necrosis factor and convert this cytokine into a soluble state. Bax *et al.* [18] suggested that the interaction of *ADAM17* with integrin $\alpha 5 \beta 1$ may target or modulate its proteolytic activity. In the spots corresponding to clusters 10 and 11, small solid structures were predominant, with a tumor-to-stroma ratio of 1:1. Infiltration of the stroma by mononuclear cells within these clusters was approximately 10%. In cluster 10, the expression of two pairs, *ADAM9*-*ITGB5* and secreted phosphoprotein 1 (*SPP1*)-*ITGA9*, and in cluster 11, that of only one pair, laminin subunit beta-3 (*LAMB3*)-*ITGB3*, was observed. In the tumor loci corresponding to clusters 13 and 14, the spots were located in two morphologically distinct regions. Approximately 25% of the spots were located in the projection of a large solid structure, and the rest in the projection of small solid, trabecular, and torpedo-like structures, with a tumor-to-stroma ratio of 1:1. TIL infiltration was 5–20%. Spots in cluster 13 showed expression of the *ITGA2* subunit, for which four ligands are indicated, three of which,

Table 1. Representation of receptor-ligand pairs in breast cancer samples.

Sample	Cluster	Integrin receptor	Ligand		References	Tumor-stroma ratio	Predominant types of morphological structures
1	0	*ITGA6*	*THBS1*	Thrombospondin 1	[11]	1:1	trabecular
			MDK	Midkine	[12]		
			LAMC1	Laminin subunit gamma-1	[13]		
	3	*ITGB3*	*MFGE8*	Milk fat globule-EGF factor 8 protein	[14]	5:1	small solid
	7	*ITGAV* *ITGA2*	*COL4A3*	Collagen alpha-3(IV) chain	[15,16]	1:1	trabecular and torpedo-like
		ITGB8	*TGFB2*	Transforming growth factor-beta 2	[17]		
	8	*ITGAV*	*CALR*	Calreticulin	No data	1:1 10:1	small solid solid
	9	*ITGB1*	*ADAM17*	Disintegrin and metalloproteinase domain 17	[18]	5:1	small solid
	10	*ITGB5*	*ADAM9*	Disintegrin and metalloproteinase domain-containing protein 9	No data	1:1	small solid
		ITGA9	*SPP1*	Secreted phosphoprotein 1	No data		
	11	*ITGB3*	*LAMB3*	Laminin subunit beta-3	No data	1:1	small solid
	13	*ITGA2*	*COL4A1*	Collagen alpha-1(IV) chain	No data	1:1	large solid, small solid, trabecular, and torpedo-like
			LAMC1	Laminin subunit gamma-1	No data		
			COL7A1	Collagen alpha-1(VII) chain	No data		
			HSPG2	Heparan sulfate proteoglycan 2	[19]		
	14	*ITGAM*	*ICAM1*	Intercellular adhesion molecule 1	[20]	1:1	small solid, trabecular, and torpedo-like
2	2	*ITGB1*	*COL4A4*	Collagen alpha-1(IV) chain	No data	50:1	solid
	6	*ITGB4*	*LAMA1*	Laminin subunit alpha-1	[21]	10:1	solid
		ITGB4	*LAMB3*	Laminin subunit beta-3	No data		
		ITGA2			No data		
		ITGA6			[22]		
		ITGA3			No data		
		ITGAV	*FGG*	Fibrinogen gamma chain	No data		

Table 1. Continued.

Sample	Cluster	Integrin receptor	Ligand		References	Tumor-stroma ratio	Predominant types of morphological structures
3	0	*ITGA3*	*PLAU*	Plasminogen activator, urokinase	[23]	1:5	trabecular
	2	*ITGB5*	*LTBP1*	Latent-transforming growth factor beta-binding protein 1	No data	1:5	trabecular
			SERPINE1	Plasminogen activator inhibitor 1 RNA-binding protein	No data		
		ITGB1	*THBS1*	Thrombospondin 1	[24]		
			COL4A5	Collagen alpha-5(IV) chain	No data		
		ITGAV	*SERPINE1*	Plasminogen activator inhibitor 1 RNA-binding protein	[25]		
	7	*ITGB4*	*LAMA5*	Laminin subunit alpha-5	[26]	1:2	trabecular
4	2	*ITGA2*	*TNC*	Tenascin C	[27]	1:5	trabecular, groups of cells
			COL6A2	Collagen alpha-2(VI) chain	[28]		
			MMP1	Matrix metalloproteinase-1	[29,30]		
	5	*ITGB1*	*ADAM2*	Disintegrin and metalloproteinase domain-containing protein 2	No data	1:5	trabecular-like, groups of cells
			MDK	Midkine is a heparin-binding growth factor	[31]		
			THBS2	Thrombospondin-2	[32]		
			COL6A2	Collagen alpha-2(VI) chain	No data		
	7	*ITGB1*	*LAMC3*	Laminin subunit gamma-3	No data	1:5	trabecular-like, groups of cells
5	2	*ITGB4*	*LAMA5*	Laminin subunit alpha-5	[26]	3:1	solid
	4	*ITGA2B*	*COL2A1*	Collagen alpha-1(II) chain	No data	3:1	solid
	5	*ITGB4* *ITGA2*	*LAMC3*	Laminin subunit gamma-3	No data	1:2	solid
			COL6A1	Collagen alpha-1(VI) chain	No data	2:1	solid
	7	*ITGA2*	*COL3A1*	Collagen alpha-1(III) chain	No data		
			COL1A1	Collagen alpha-1(I) chain	[33]		

ITGA6, integrin alpha 6; *ITGB3*, integrin beta 3.

namely, *COL4A1*, *LAMC1* and heparan sulfate proteoglycan 2 (*HSPG2*) encode basal membrane proteins. However, the functional relationship between the proteins encoded by *ITGA2* and these ligands is poorly understood. However, based on the general patterns of interaction of integrins with the basal membrane, which provides anchorage-dependent cell survival, external stimulus transduction that activates signaling pathways and corresponding functional changes in cells, similar effects can be expected from integrin $\alpha 2$, which binds the aforementioned proteins of the basal membrane. Cluster 14 was characterized by the expression of the intercellular adhesion molecule 1 (*ICAM1*)-*ITGAM* ligand-receptor pair.

In the second sample, the spots in cluster 2 were located in the projection of solid structures. The tumor-to-stroma ratio was 50:1. The presence of stroma in regions of the tumor was represented by coarse fibrous connective tissue. In the tumor sample from the second patient, cluster 2 was identified based on the *COL4A4-ITGB1* functional relationship. Integrin $\beta 1$ subunit as part of $\alpha 1\beta 1$, $\alpha 2\beta 1$, $\alpha 10\beta 1$, and $\alpha 11\beta 1$ heterodimers is known to bind collagens. *COL4A4* encodes one of the six subunits of type IV collagen, a major structural component of basal membranes. Cluster 6 spots were located in the projections of the solid tumoral structures. The tumor-stroma ratio was 10:1, and TIL infiltration was approximately 10%. The stromal component was represented by coarse fibrous connective tissue. Cluster 6 was characterized by the associative expression of four genes namely, α - *ITGA2*, *ITGA3*, *ITGA6* and *ITGAV* and one βsubunit, *ITGB4*. The ligands for the products of all subunit genes except *ITGAV* are basal membrane laminin proteins, which are encoded by laminin subunit alpha-1 (*LAMA1*) and *LAMB3*.

In cluster 0 of the third sample, the stroma was predominant, represented by coarse fibrous connective tissue, and the tumor-to-stroma ratio was 1:5. Trabecular structures were predominant in the tumor and the projection of spots belonging to cluster 0. TIL infiltration was approximately 5%. Cluster 0 was represented by only one ligand-receptor pair, plasminogen activator, urokinase (*PLAU*)-*ITGA3*. Cluster 2 was mainly represented by coarse fibrous connective tissue with a tumor-stroma ratio of 1:5. Trabecular structures predominated in the tumor and the projection of spots belonging to cluster 2, whereas TIL infiltration was approximately 5%. Cluster 2 was characterized by the widest range of interactions: latent-transforming growth factor beta-binding protein (*LTBP1*)-*ITGB5*, plasminogen activator inhibitor 1 RNA-binding protein (*SERPINE1*)-*ITGB5*, *THBS1-ITGB1*, *COL4A5-ITGB1*, *SERPINE1-ITGAV*; cluster 7 revealed only one ligand-receptor pair, *LAMA5-ITGB4*, which is associated with resistance to apoptosis and anchor-independent survival [35].

Clusters 2 and 5 in the fourth sample were represented by small trabecular-like structures and groups of cells. The tumor-to-stroma ratio was 1:5, and TIL infiltration was 5-10%. Cluster 7 was dominated by small trabecular-like structures and groups of cells. The stroma was partially represented by bundles of smooth muscle fibers. The tumor-stroma ratio was 1:5, and the TIL infiltration was –5-10%. The peculiarity of the fourth sample was that only one integrin subunit was detected in each of the three clusters with the simultaneous expression of multiple ligands. *ITGA2* expression was detected in cluster 2, whereas that of *ITGB1* was detected in clusters 5 and 7. Three ligands of *ITGA2* were detected in cluster 2—tenascin C (*TNC*), *COL6A2*, and matrix metalloproteinase-1 (*MMP1*). Ligands of *ITGB1—ADAM2*, *MDK*, *THBS2*, *COL6A2*—were detected in cluster 5, and in cluster 7, expression of *LAMC3* was detected.

All tumor clusters in the fifth sample were represented by carcinoma cells with significant predominance of solid structures. However, the tumor-stroma ratio varied significantly: in clusters 2 and 4 it was 3:1, in cluster 5 it was 1:2, and in cluster 7 it was 2:1. The stromal TIL infiltration was approximately 5%. The *LAMA5-ITGB4* pair was detected in cluster 2. Cluster 4 was characterized by *COL2A1-ITGA2B* expression. In cluster 5, two integrin pairs with the same ligand, *LAMC3-ITGB4* and *LAMC3-ITGA2*, were found, whereas in cluster 7 showed, three pairs involving the same integrin but different ligands, *COL6A1-ITGA2*, *COL3A1-ITGA2*, *COL1A1-ITGA2*.

Thus, intratumoral heterogeneity manifested by the presence of several morphological loci was associated with the integrin-ligand functional clusters in each histological tumor sample. Inter-tumoral heterogeneity was manifested by a different number of functional clusters, ranging from 2 to 9 in each tumor sample.

An unexpected result obtained was the rarity of the presence of complementary α and β subunits in the same cluster capable of forming heterodimeric integrins. Only five potential heterodimeric integrins were identified in these four tumor samples. The expression of subunits capable of forming these five heterodimeric integrins in a single cell is highly probable. Indeed, the data presented in Table 2 indicate the expression of the integrin subunits found in a single spot.

The main characteristic of these clusters was the significantly predominant expression of non-complementary integrin subunits. Of the 42 functional integrin-ligand pairs in 21 clusters of five samples, 41 pairs occurred only once. The exception was the *LAMA5-ITGB4* pair, which was detected in two clusters of different samples.

Discussion

Diverse manifestations of heterogeneity in breast cancer have been studied, which complicate early diagnosis, selection of treatment strategies, and prediction of prognosis [3,36]. We evaluated functional ligand-receptor interactions in tumor cells, with respect to the heterogeneity of

Table 2. Presence of complementary subunits of integrins in breast cancer samples.

Samples	Number of clusters with tumor cells	α-subunits	β-subunits	Complementary subunits of integrins in the cluster (potential heterodimers)	Number of cluster spots with co-expression
1	9	*ITGA6*, *ITGAV*, *ITGA2*, *ITGA9*, *ITGAM*	*ITGB1*, *ITGB3*, *ITGB5*, *ITGB8*	Cluster7 *ITGAV-ITGB8*	182/206
2	2	*ITGAV*, *ITGA2*, *ITGA3*, *ITGA6*	*ITGB1*, *ITGB4*	Cluster 6 *ITGA6-ITGB4*	64/174
3	3	*ITGA3*, *ITGAV*	*ITGB1*, *ITGB4*, *ITGB5*	Cluster 2 *ITGAV-ITGB1* *ITGAV-ITGB5*	335/379 323/379
4	3	*ITGA2*	*ITGB1*	-	
5	4	*ITGA2*, *ITGA2B*	*ITGB4*	Cluster 5 *ITGA2-ITGB4*	16/340

breast cancer. Only spots containing tumor cells were included in the NICHES analysis. Tumor cells and stroma were present in different proportions in each spot, with different numbers of mononuclear leukocytes constituting the tumor microenvironment. This would be expected if leukocyte integrins accounted for a significant proportion of functional integrin-ligand pairs in the clusters. Integrins expressed predominantly by leukocytes are considered to consist of the β2 subunit, which can form heterodimers αLβ2, αMβ2, αXβ2, and αDβ 2 or the α4 subunit forming heterodimeric integrins α4β1 and α4β7 [37]. However, it turned out that neither the β2 nor α4 subunit was present among the integrins of the clusters obtained. This result is remarkable and suggests that the functionally relevant integrin-ligand pairs detected in each cluster preferentially reflect the functional potency of the tumor cells. The tumor tissue samples studied were represented by different multicellular structures: tubular, trabecular, torpedo-like, solid, and groups of cells. The data we previously obtained indicate the prognostic value of some of these markers in patients with breast cancer [5]. It appears that the clusters identified based on ligand-receptor cell-cell interactions did not vary depending on the morphology of tumors. In this context, the heterogeneity observed in integrin-ligand pairs, as revealed from our study, appears to be spatial rather than linked to morphological structures. Moreover, compelling evidence has emerged that highlights the divergent nature of morphological and spatial heterogeneity. Consequently, the functional status of a particular tumor site reflects a combination of morphological and spatial heterogeneity. Spatial heterogeneity is characterized by differences between tumor regions at the phenotypic, transcriptomic, epigenetic, and genomic levels [38]. It is necessary to compare the nature of spatial heterogeneity of tumors with the functional mosaicism of parenchymatous organs such as healthy liver tissue [39]. The functional activity of tumors varies regionally from high to low over time, and vice versa.

Inter-tumoral morphological heterogeneity was also highly pronounced, as exhibited by the predominance of varying structures formed by tumor cells. Spatial inter-tumoral heterogeneity was characterized by a unique set of clusters ranging in number from two to nine, with each cluster encompassing different integrin-ligand cell-cell interactions. Concurrently, nearly all integrin-ligand pairs exhibited minimal recurrence, except for *ITGB4-LAMA5*. The uniqueness of these pairs was owing to the difference in ligands for the same integrin; the most frequently found integrins were *ITGB1* and *ITGA2*. High *ITGB1* expression is associated with poor overall survival (OS) in breast cancer [40]. Furthermore, in the mouse model, integrin β1 has been shown to play a key role in bone colonization in breast cancer [41], while in vitro experiments describe mechanisms of chemoresistance, inhibition of cell growth and promotion of cell survival in circulation [42,43].

Clinical data on the association of integrin α2 with breast cancer prognosis are inadequate; however, experimental evidence suggests its significant contribution to cell adhesion, cell motility, angiogenesis, and stemness properties [44]. High expression of integrins β1 and α2 is associated with EMT [45]. Interestingly, these subunits can form an integrin α2β1 dimer, which is being considered as a target for breast cancer therapy, particularly with Aspartic Acid-Glycine-Glutamic Acid-Alanine (DGEA)-modified liposomal doxorubicin [46]. Half of the interactions observed in the study were predicted theoretically, and there are no experimental data confirming these interactions. The role of the axis of integrin β4 with various laminins as ligands in tumor progression and metastasis has been studied most [47,48]. The integrin signaling pathway activated by laminins regulates various forms of cell death, including anoikis, autophagy, entosis, and cell cycle arrest, thereby ensuring anchorage-independent cell survival [49]. Moreover, tumor cells can adapt to the loss of adhesion to the basal membrane and avoid anoikis through α6β4-mediated adhesion to autocrine-produced laminin. Consequently, these tumor cells acquire the ability to grow inde-

pendent of their attachment to the basal membrane. Notably, the interaction of *ITGB4* with various laminins was the most frequent in the studied clusters.

Notably, most of the tumor loci studied were characterized by the expression of integrin subunit genes, which are not capable of forming heterodimers. There are no experimental data on expression of isolated integrin subunits on the cell surface. There is a study showing that each subunit of the αMβ2 heterodimer has different properties and that the function of the αMβ2 heterodimer is a composite of the functions of its individual subunits [50]. Examination of the functional implications of the isolated subunits in carcinoma progression requires dedicated and specialized investigations.

In our study, only five pairs of complementary integrin subunits with the potential to form heteromeric integrins were identified in the same cluster spot. The complementary subunits, *ITGAV* and *ITGB8*, were detected in the first patient sample, in one of the nine clusters in 182/206 spots, and therefore, we were able to predict the possible formation of a heterodimer of integrin αVβ8, the receptor for fibronectin. The functional significance of this interaction may be similar to that of αvβ3 integrin, increased expression of which contributes to the effects of transforming growth factor beta (TGF-β) mediated induction of EMT [51]. *ITGA6-ITGB4* pairing was detected in cluster 6 of the second sample. The presence of two complementary subunits of *ITGA6* and *ITGB4* in 64/174 spots suggests the possibility of formation of a heterodimeric integrin α6β4.

The spatial heterogeneity of integrin-ligand expression clusters in breast cancer contributes significantly to the integral functional heterogeneity of the tumor, which sets the stage for many scenarios of parenchymatous-stromal relationships, some of which may be effective in the emergence of metastasizing tumor seed cells.

Our discovery of intra- and inter-tumoral spatial functional heterogeneity of the tumor tissue may largely explain why it is difficult to achieve success in most patients using any therapeutic strategy targeting any particular molecule, irrespective of the importance of its pathogenetic significance.

Conclusions

Luminal breast cancer is characterized by marked inter- and intra-tumoral heterogeneity in the expression profiles of integrins and their ligands. This heterogeneity was not related to morphological heterogeneity and reflected the spatial heterogeneity of the tumor. In the future, functional interpretation of such variants of parenchymatous-stromal relationships characterized by specific integrin-receptor pairs will provide flexibility in the search for therapeutic targets.

Availability of Data and Materials

GEO Database: GSE242311.

Author Contributions

Conceived and designed the analysis: LT and VP; acquired the data: EG and VA; performed the analysis: PI and MZ; wrote the article: LT, EG, VA and PI; critical revision: MZ and VP. All authors have read and approved the final manuscript and agreed to be accountable for all aspects of the work.

Ethics Approval and Consent to Participate

The Institutional Review Board (IRB) of the Cancer Research Institute, Tomsk National Research Medical Center, approved the study in accordance with good clinical practice guidelines and the Declaration of Helsinki (local IRB approval: August 25, 2020, number 7). All the patients signed an informed consent form to participate in the study.

Acknowledgment

Not applicable.

Funding

The study was supported by the Russian Science Foundation (grant #21-15-00140).

Conflict of Interest

The authors declare no conflict of interest.

Supplementary Material

Supplementary material associated with this article can be found, in the online version, at https://doi.org/10.24976/Discov.Med.202335178.86.

References

[1] Mezu-Ndubuisi OJ, Maheshwari A. The role of integrins in inflammation and angiogenesis. Pediatric Research. 2021; 89: 1619–1626.

[2] Valdembri D, Serini G. The roles of integrins in cancer. Faculty Reviews. 2021; 10: 45.

[3] Guo L, Kong D, Liu J, Zhan L, Luo L, Zheng W, *et al*. Breast cancer heterogeneity and its implication in personalized precision therapy. Experimental Hematology & Oncology. 2023; 12: 3.

[4] Kashyap A, Rapsomaniki MA, Barros V, Fomitcheva-Khartchenko A, Martinelli AL, Rodriguez AF, *et al*. Quantification of tumor heterogeneity: from data acquisition to metric generation. Trends in Biotechnology. 2022; 40: 647–676.

[5] Zavyalova MV, Denisov EV, Tashireva LA, Gerashchenko TS, Litviakov NV, Skryabin NA, *et al*. Phenotypic drift as a cause

for intratumoral morphological heterogeneity of invasive ductal breast carcinoma not otherwise specified. BioResearch Open Access. 2013; 2: 148–154.

[6] Hao Y, Hao S, Andersen-Nissen E, Mauck WM, Zheng S, Butler A, *et al*. Integrated analysis of multimodal single-cell data. Cell. 2021; 184: 3573–3587.

[7] Hafemeister C, Satija R. Normalization and variance stabilization of single-cell RNA-seq data using regularized negative binomial regression. Genome Biology. 2019; 20: 296.

[8] Raredon MSB, Yang J, Kothapalli N, Lewis W, Kaminski N, Niklason LE, *et al*. Comprehensive visualization of cell-cell interactions in single-cell and spatial transcriptomics with NICHES. Bioinformatics (Oxford, England). 2023; 39: btac775.

[9] Linderman GC, Zhao J, Roulis M, Bielecki P, Flavell RA, Nadler B, *et al*. Zero-preserving imputation of single-cell RNA-seq data. Nature Communications. 2022; 13: 192.

[10] Saiselet M, Rodrigues-Vitória J, Tourneur A, Craciun L, Spinette A, Larsimont D, *et al*. Transcriptional output, cell-type densities, and normalization in spatial transcriptomics. Journal of Molecular Cell Biology. 2020; 12: 906–908.

[11] Wu Y, Tan X, Liu P, Yang Y, Huang Y, Liu X, *et al*. ITGA6 and RPSA synergistically promote pancreatic cancer invasion and metastasis via PI3K and MAPK signaling pathways. Experimental Cell Research. 2019; 379: 30–47.

[12] Campbell WA, Fritsch-Kelleher A, Palazzo I, Hoang T, Blackshaw S, Fischer AJ. Midkine is neuroprotective and influences glial reactivity and the formation of Müller glia-derived progenitor cells in chick and mouse retinas. Glia. 2021; 69: 1515–1539.

[13] Ramadan R, Wouters VM, van Neerven SM, de Groot NE, Garcia TM, Muncan V, *et al*. The extracellular matrix controls stem cell specification and crypt morphology in the developing and adult mouse gut. Biology Open. 2022; 11: bio059544.

[14] Deroide N, Li X, Lerouet D, Van Vré E, Baker L, Harrison J, *et al*. MFGE8 inhibits inflammasome-induced IL-1β production and limits postischemic cerebral injury. The Journal of Clinical Investigation. 2013; 123: 1176–1181.

[15] Wang H, Su Y. Collagen IV contributes to nitric oxide-induced angiogenesis of lung endothelial cells. American Journal of Physiology-Cell Physiology. 2011; 300: C979–C988.

[16] Rubel D, Frese J, Martin M, Leibnitz A, Girgert R, Miosge N, *et al*. Collagen receptors integrin alpha2beta1 and discoidin domain receptor 1 regulate maturation of the glomerular basement membrane and loss of integrin alpha2beta1 delays kidney fibrosis in COL4A3 knockout mice. Matrix Biology. 2014; 34: 13–21.

[17] Worthington JJ, Kelly A, Smedley C, Bauché D, Campbell S, Marie JC, *et al*. Integrin αvβ8-Mediated TGF-β Activation by Effector Regulatory T Cells Is Essential for Suppression of T-Cell-Mediated Inflammation. Immunity. 2015; 42: 903–915.

[18] Bax DV, Messent AJ, Tart J, van Hoang M, Kott J, Maciewicz RA, *et al*. Integrin alpha5beta1 and ADAM-17 interact in vitro and co-localize in migrating HeLa cells. The Journal of Biological Chemistry. 2004; 279: 22377–22386.

[19] Woodall BP, Nyström A, Iozzo RA, Eble JA, Niland S, Krieg T, *et al*. Integrin alpha2beta1 is the required receptor for endorepellin angiostatic activity. The Journal of Biological Chemistry. 2008; 283: 2335–2343.

[20] Yuan Z, Yan K, Wang J. Overexpression of integrin β_2 improves migration and engraftment of adipose-derived stem cells and augments angiogenesis in myocardial infarction. Annals of Translational Medicine. 2022; 10: 863.

[21] Islam K, Thummarati P, Kaewkong P, Sripa B, Suthiphongchai T. Role of laminin and cognate receptors in cholangiocarcinoma cell migration. Cell Adhesion & Migration. 2021; 15: 152–165.

[22] Béguin EP, Janssen EFJ, Hoogenboezem M, Meijer AB, Hoogendijk AJ, van den Biggelaar M. Flow-induced Reorganization of Laminin-integrin Networks Within the Endothelial Basement Membrane Uncovered by Proteomics. Molecular & Cellular Proteomics. 2020; 19: 1179–1192.

[23] Zou B, Li J, Xu K, Liu JL, Yuan DY, Meng Z, Zhang B. Identification of key candidate genes and pathways in oral squamous cell carcinoma by integrated Bioinformatics analysis. Experimental and Therapeutic Medicine. 2019; 17: 4089–4099.

[24] Xu ZY, Chen JS, Shu YQ. Gene expression profile towards the prediction of patient survival of gastric cancer. Biomedicine & Pharmacotherapy. 2010; 64: 133–139.

[25] Dai W, Xiao Y, Tang W, Li J, Hong L, Zhang J, *et al*. Identification of an EMT-Related Gene Signature for Predicting Overall Survival in Gastric Cancer. Frontiers in Genetics. 2021; 12: 661306.

[26] Englund JI, Ritchie A, Blaas L, Cojoc H, Pentinmikko N, Döhla J, *et al*. Laminin alpha 5 regulates mammary gland remodeling through luminal cell differentiation and Wnt4-mediated epithelial crosstalk. Development (Cambridge, England). 2021; 148: dev199281.

[27] Karkampouna S, De Filippo MR, Ng CKY, Klima I, Zoni E, Spahn M, *et al*. Stroma Transcriptomic and Proteomic Profile of Prostate Cancer Metastasis Xenograft Models Reveals Prognostic Value of Stroma Signatures. Cancers. 2020; 12: 3786.

[28] Yang J, Hou Z, Wang C, Wang H, Zhang H. Gene expression profiles reveal key genes for early diagnosis and treatment of adamantinomatous craniopharyngioma. Cancer Gene Therapy. 2018; 25: 227–239.

[29] Zhou H, Xiang Q, Hu C, Zhang J, Zhang Q, Zhang R. Identification of MMP1 as a potential gene conferring erlotinib resistance in non-small cell lung cancer based on bioinformatics analyses. Hereditas. 2020; 157: 1–10.

[30] Foki E, Gangl K, Kranebitter V, Niederberger-Leppin V, Eckl-Dorna J, Wiebringhaus R, *et al*. Early effects of cigarette smoke extract on human oral keratinocytes and carcinogenesis in head and neck squamous cell carcinoma. Head & Neck. 2020; 42: 2348–2354.

[31] Kinoshita D, Shishido T, Takahashi T, Yokoyama M, Sugai T, Watanabe K, *et al*. Growth Factor Midkine Aggravates Pulmonary Arterial Hypertension via Surface Nucleolin. Scientific Reports. 2020; 10: 10345.

[32] Qi L, Sun B, Yang B, Lu S. CEBPB regulates the migration, invasion and EMT of breast cancer cells by inhibiting THBS2 expression and O-fucosylation. Human Molecular Genetics. 2023; 32: 1850–1863.

[33] Rattanasinchai C, Navasumrit P, Ruchirawat M. Elevated ITGA2 expression promotes collagen type I-induced clonogenic growth of intrahepatic cholangiocarcinoma. Scientific Reports. 2022; 12: 22429.

[34] Dieci MV, Radosevic-Robin N, Fineberg S, van den Eynden G, Ternes N, Penault-Llorca F, *et al*. Update on tumor-infiltrating lymphocytes (TILs) in breast cancer, including recommendations to assess TILs in residual disease after neoadjuvant therapy and in carcinoma in situ: A report of the International Immuno-Oncology Biomarker Working Group on Breast Cancer. Seminars in Cancer Biology. 2018; 52: 16–25.

[35] Weaver VM, Lelièvre S, Lakins JN, Chrenek MA, Jones JCR, Giancotti F, *et al*. beta4 integrin-dependent formation of polarized three-dimensional architecture confers resistance to apoptosis in normal and malignant mammary epithelium. Cancer Cell. 2002; 2: 205–216.

[36] Fumagalli C, Barberis M. Breast Cancer Heterogeneity. Diagnostics (Basel, Switzerland). 2021; 11: 1555.

[37] Hyun YM, Lefort CT, Kim M. Leukocyte integrins and their ligand interactions. Immunologic Research. 2009; 45: 195–208.

[38] Vogelstein B, Papadopoulos N, Velculescu VE, Zhou S, Diaz LA, Jr, Kinzler KW. Cancer genome landscapes. Science (New

York, N.Y.). 2013; 339: 1546–1558.

[39] Holzhütter HG, Berndt N. Computational Hypothesis: How Intra-Hepatic Functional Heterogeneity May Influence the Cascading Progression of Free Fatty Acid-Induced Non-Alcoholic Fatty Liver Disease (NAFLD). Cells. 2021; 10: 578.

[40] Sun Q, Zhou C, Ma R, Guo Q, Huang H, Hao J, *et al*. Prognostic value of increased integrin-beta 1 expression in solid cancers: a meta-analysis. OncoTargets and Therapy. 2018; 11: 1787–1799.

[41] Thibaudeau L, Taubenberger AV, Theodoropoulos C, Holzapfel BM, Ramuz O, Straub M, *et al*. New mechanistic insights of integrin β1 in breast cancer bone colonization. Oncotarget. 2015; 6: 332–344.

[42] Baltes F, Pfeifer V, Silbermann K, Caspers J, Wantoch von Rekowski K, Schlesinger M, *et al*. β1-Integrin binding to collagen type 1 transmits breast cancer cells into chemoresistance by activating ABC efflux transporters. Biochimica et Biophysica Acta. Molecular Cell Research. 2020; 1867: 118663.

[43] Hou S, Isaji T, Hang Q, Im S, Fukuda T, Gu J. Distinct effects of β1 integrin on cell proliferation and cellular signaling in MDA-MB-231 breast cancer cells. Scientific Reports. 2016; 6: 18430.

[44] Adorno-Cruz V, Liu H. Regulation and functions of integrin α2 in cell adhesion and disease. Genes & Diseases. 2018; 6: 16–24.

[45] Wafai R, Williams ED, de Souza E, Simpson PT, McCart Reed AE, Kutasovic JR, *et al*. Integrin alpha-2 and beta-1 expression increases through multiple generations of the EDW01 patient-derived xenograft model of breast cancer-insight into their role in epithelial mesenchymal transition in vivo gained from an in vitro model system. Breast Cancer Research. 2020; 22: 136.

[46] Zhou B, Li M, Xu X, Yang L, Ye M, Chen Y, *et al*. Integrin α_2β_1 Targeting DGEA-Modified Liposomal Doxorubicin Enhances Antitumor Efficacy against Breast Cancer. Molecular Pharmaceutics. 2021; 18: 2634–2646.

[47] Hao N, Yang D, Liu T, Liu S, Lu X, Chen L. Laminin-integrin a6b4 interaction activates notch signaling to facilitate bladder cancer development. BMC Cancer. 2022; 22: 558.

[48] Yang H, Xu Z, Peng Y, Wang J, Xiang Y. Integrin β4 as a Potential Diagnostic and Therapeutic Tumor Marker. Biomolecules. 2021; 11: 1197.

[49] Deng Z, Wang H, Liu J, Deng Y, Zhang N. Comprehensive understanding of anchorage-independent survival and its implication in cancer metastasis. Cell Death & Disease. 2021; 12: 629.

[50] Solovjov DA, Pluskota E, Plow EF. Distinct roles for the alpha and beta subunits in the functions of integrin alphaMbeta2. The Journal of Biological Chemistry. 2005; 280: 1336–1345.

[51] Kariya Y, Oyama M, Suzuki T, Kariya Y. αvβ3 Integrin induces partial EMT independent of TGF-β signaling. Communications Biology. 2021; 4: 490.